Universidad de La Laguna
Facultad de Ciencias
Grado en Física

Trabajo de Fin de Grado

Sensitivity study for optical sensors based on resonant modes.

Autora
Nayra Machín Padrón

Tutores
Susana Rios Rodríguez
Inocencio R. Martin Benenzuela

Julio 2023

Contents

Abstract

This bachelor thesis consists on a theoretical study of the sensitivity of an optical sensor, based on the Whispering Gallery Modes (WGM) of an optical resonator, through numerical simulations. The resonators under study are glass microspheres. Specifically, a displacement in wavelength of the resonant modes of the sphere is expected due to a variation in the refractive index of the external medium related to a change in temperature or composition. The optical sensor will be characterized to determinate its sensitivity. Physics behind Whispering Gallery Modes resonators is going to be studied with the purpose of optimizing the sensor. This project aims to provide some basis to the development high sensitive optical sensors based on resonant modes.

Summary

Este trabajo de fin de grado enfocado en la detección óptica consiste en un estudio teórico de la sensibilidad de un resonador óptico concreto utilizado como sensor. La investigación se realizará mediante modelizaciones numéricas que permitan comprender y analizar la respuesta del resonador frente a cambios en variables físicas del entorno.

El resonador bajo estudio es un microesfera de vidrio sensible a cambios en el medio externo. Factores como la temperatura producen un cambio de indice de refracción del medio. Como consecuencia de los cambios en el índice de refracción, los modos resonantes de la esfera sufren un desplazamiento en longitud de onda. El objetivo es observar y cuantificar dicho desplazamiento para caracterizar el sensor en términos de su sensibilidad a dichos cambios. Esta memoria incluye una revisión de los principios físicos asociados a los modos resonantes de una esfera denominados *Whispering Gallery Modes* (WGM) y del *scattering* Mie. Este estudio proporciona una base teórica que permite abordar el diseño óptimo de sensores ópticos basados en modos de resonancia.

Para llevar a cabo este estudio teórico y simular el funcionamiento del sensor, se han desarrollado códigos en Python, cuyo objetivo es el cálculo de los modos resonantes de una esfera basados en dos métodos numéricos bien establecidos: el método de Schiller y el algoritmo de Bohren-Huffman. El método de Schiller que es una aproximación la resolución de la ecuación de Helmholtz que deriva en los modos ópticos TE y TM y proporciona información sobre la longitud de onda resonante de un modo óptico específico caracterizado por dos números (n y l) que etiquetan la componente radial y polar del modo, respectivamente. Por otro lado, el algoritmo de Bohren-Huffman se basa en el scattering Mie concretamente en el cálculo del coeficiente de extinción para determinar la posición de las resonancias de una forma más exacta.

El proceso de simulación involucra la exploración de diversas configuraciones de índices de refracción para el vidrio de las microesferas y para el medio externo. Se busca determinar la diferencia de índices de refracción que permita maximizar la sensibilidad del sensor, es decir, produci un desplazamiento apreciable de los modos resonantes para valores pequeños de las variaciones de temperatura o composición del medio externo. El estudio también abarca la influencia del tamaño de las microesferas en los modos resonantes. Se llevará a cabo un análisis detallado para determinar los rangos apropiados de tamaño de las microesferas que optimizan la respuesta del sensor. Además, se analizará la estructura ondulante del coeficiente de extinción, lo cual proporciona una comprensión más profunda de los fenómenos ópticos involucrados en la interacción entre el resonador y el entorno.

1 Introduction

En esta sección se contextualiza el problema tratado en este trabajo de fin de grado y se nombran algunos de los últimos avances relacionados con el campo de los sensoses basados en modos resonantes y su sensibilidad. A continuación se detallan a grandes rasgos los contenidos del trabajo, que está centrado en el estudio teórico de la sensibilidad de un resonador óptico utilizado como sensor. Se describe cómo se utilizarán simulaciones basadas en métodos numéricos de estimación para estudiar el comportamiento de microesferas de vidrio, sensibles a cambios en el medio externo produciendo un desplazamiento de los modos resonantes como respuesta. Se estudiarán los principios físicos tras los modos resonantes con el objetivo de encontrar la configuración óptima de medios materiales y tamaño de la esfera para dicho sensor. Y finalmerte se realizará un estudio de la sensibilidad además de una discusión de la estructura ondulante que posee el coeficiente de extinción de una esfera iluminada.

Optical resonators are devices that have resonance phenomena of light within a cavity; this happens by total internal reflection or by forming a resonant cavity in a dielectric material. This interaction between light and the surrounding matter can be used for sensing purposes. Optical resonators have shown high sensitivity for detecting changes in the refractive index of the surrounding medium. Some of the recent research studies on the sensitivity of optical sensors based on resonant modes are listed below.

Experimental studies have shown that the sensitivity of a Fabry-Perot resonance mode sensor can be up to the order of 10^{-5}, much higher than typical evanescent field sensors sensitivity [1]. Another study used a double-layer resonant meta-grating structure to improve the sensitivity of refractive index sensors. The study found that the sensitivity of the sensor is determined by the interaction between the resonant mode and the analyte [2]. Lossy-mode resonance (LMR)–based optical sensing technology has emerged as a nanotechnological platform with very high sensitivity. LMR devices can be sensitive to the refractive index and thickness of the thin film and to the surrounding-medium refractive index as well [3]. A study proposed a design tool for dielectric optical resonator-based biochemical refractometry sensors and introduced a new sensor system figure of merit, the time-normalized sensitivity, to allow a quantitative comparison between resonator sensors with distinctive device designs and configurations. The study found that the time-normalized sensitivity critically depends on the cavity Q-factor, and developed a method of optimizing sensor resolution and sensitivity to noise as a function of cavity Q-factor [4].

Overall, the sensitivity of optical sensors based on resonant modes can be improved by optimizing the design of the sensor, the materials used and the detection mechanism.

This bachelor's thesis is focused on glass microspheres as the resonator chosen, they are sensitive to changes in the surrounding medium. Factors such as temperature or concentration of certain substances in the environment can cause a refractive index change in the medium where the microspheres are immersed. The objective is to observe and quantify the shift of the microsphere's resonant modes in response to these changes in refractive index, allowing the characterization of the sensor in terms of sensitivity. A review of the physical principles associated with Whispering Gallery Mode resonances and Mie scattering is included, focusing on how they influence the sensor's performance and its sensitivity with the aim of its optimization. To carry out this theoretical study and simulate the sensor's behavior, Python codes have been developed for calculating resonance modes of a sphere they are based on two numerical methods: the Schiller method and the Bohren-Huffman algorithm. The Schiller method, which is an approximation of the Helmholtz equation solution that results in the TE and TM optical

modes, provides information about the resonant wavelength of a specific optical mode characterized by two numbers (n and l) representing the radial and polar components of the mode, respectively. On the other hand, the Bohren-Huffman algorithm is based on the concept of Mie scattering and the study of the extinction coefficient to determine the resonance positions more accurately through its graphic representation. The simulation involves exploring various refractive configurations for the microsphere's glass and the surrounding medium. The aim is to determine the optimal refractive index difference that allows for favorable sensor performance, having a shift in the resonance modes for small values of temperature or external media composition. The study also covers the influence of microsphere size on resonant modes, leading to an analysis to determine the ranges of size that optimize the response of the sensor. Additionally, a discussion on the ripple structure of the extinction efficiency is carried out, providing a deeper understanding of the optical phenomena involved in the interaction between the microsphere and the environment. This work will allow identifying the optimal conditions to maximize the sensitivity of the sensor in terms of its ability to detect changes in physical variables of the environment.

2 Aim of this work

En esta sección se explican los objetivos principales de este trabajo de fin de grado. El interés principal es determinar la sensibilidad de un sensor óptico cuyo principio de actuación es el desplazamiento de los modos resonantes en la cavidad debido a una variación en el índice de refracción del medio donde se situa el resonador. Se realizarán simulaciones, para un medio externo determinado, de las distintas respuestas asociadas a resonadores de distintos tamaños e índices de refracción con el objetivo de obtener una configuración que maximize la sensibilidad del sensor.

The main interest in this bachelor's thesis is to study the performance of a specific kind of optical resonator as a sensor. This sensor is based on the response of the resonant modes to a variation in the refractive index of the medium where the resonator is immersed.
To characterise the sensor performance by its sensitivity the following steps are going to be followed:

- Implement algorithms that allow computational modelling of the resonant modes inside a sphere. The parameters of interest are the size of the sphere, the refractive index of the sphere and refractive index of the surrounding medium.
- Use the algorithms to calculate the displacement of the resonant wavelengths when a variation in the refractive index of the external medium is introduced.
- Study the resonator's response in function of its size and the refractive index difference between the resonator and the external medium.
- Observe, through numerical simulations, the behaviour of the resonant modes under a variation of the parameters mentioned above. Paying special attention to the width of the modes.
- Obtain a range of values of size and refractive index difference that lead to an optimal sensitivity of the sensor.
- Summarize the main conclusions of the work.

Our final goal is to develop a highly sensitive sensor that can be used in various applications. This work will include mainly theoretical modelling and data analysis to optimise the sensor performance and discover its limitations.

3 Theoretical background

Con el propósito de comprender los objetivos y la metodología empleada en este trabajo, en este capitulo se revisarán los fundamentos teóricos de los sensores basados en modos resonantes, así como las propiedades que describen su actuación y se abordará el estudio de estos modos dentro del contexto del scattering Mie.

3.1 Sensors

Sensors are devices used to obtain quantitative information about the environment. In practice, they detect some change that is usually converted to an optical or electrical signal that can be processed. The most frequent types of sensors are used for temperature, pressure, humidity, motion and chemical composition detection. Another common type of sensors are the optical ones; they use light to detect some variation in their optical properties that is related to a change in their surroundings [5]. Optical sensors have a variety of applications in several industries; some of them are in the biomedical field [6], in electrical systems for current and magnetic field measurements [7] and for medical uses like monitoring cancer disease through the quantification of tumour cells [8], among others.

Optical sensing consists on a light source, a sensing element and a detector, where the interaction between light and the sensing element allows measuring variations on the external medium. This measure provides sensitive detection of the target variable with many applications like the ones mentioned previously. There are optical sensors based on different physical properties like fluorescence [9], absorption [10], interference [11] and whispering gallery modes [12] among others. This work is centred on the study of the sensitivity of WGM-based optical sensors.

3.2 Optical resonators

Optical resonators are devices that allow a beam of light to travel in a closed path [14]. They can be arrangements of mirrors or other optical elements that form a cavity for light waves. Light confined in the cavity reflects multiple times, producing modes with certain resonance frequencies [15]. Light wave behaviour allows optical frequencies to remain in the structure where light is confined without large losses. The stationary waves inside the cavity, which are called resonant modes are fixed in number and distribution by the geometry of the resonator and the materials they are made with [16]. These properties make them useful for different applications; optical resonators are used in lasers [17], interferometers [18] and optical parametric oscillators[19]. These applications lie on resonator's ability to generate or select waves with specific frequencies, making them useful for working as sensing elements in optics. Resonator-based sensor's performance resides on the fact that a variation on the variable under study would produce a shift in the resonance frequencies of the resonator [13]. The sensitivity of the sensor depends on the resonator's capacity to interact with its surroundings and to produce changes in resonance due to a variation in the optical properties of the medium.

3.3 Sensor performance

In order to accurately test the performance of the sensor, there are several measurable characteristics that are key for developing a high-quality sensor. These characteristics are also useful for comparing the sensor with other existing ones.

The quality factor (Q-factor) of WGMs is a measure of the energy stored in the resonator per oscillation cycle [20]. It measures of how neat the resonance is and it relates to the lifetime of the mode. For a high value of the factor, the lifetime of the mode is larger and the resonance is sharper. For optical resonators, as light is bound inside the cavity, light losses are low giving high values for the quality factor[5]. Also a high value is achieved for large index differences inside the cavity and the external medium [21]. The Q-factor of WGMs can be tuned by stretching or annealing the microsphere, which can be useful for optimising its coupling to emitters with given transition frequencies [22] [23].

Uncertainty is another feature that defines the performance of a sensor, its defined as the minimal value of temperature or concentration change that can be measured.

As pointed out in the introduction, sensitivity is an important characteristic of the sensor performance. Sensitivity refers to the change in the optical signal corresponding to a change in the analyte. It depends on various factors as the type of sensor, design, materials and detection mechanism. Some of the factors that could be improved to optimise sensitivity are the detection mechanism used, the design of the sensor and materials election. Sensitivity is also a parameter that determines the sensor's detection limit. Therefore, optimising the sensitivity of an optical sensor is essential to improve its performance [24].

The rate at which wavelength, that is the measured parameter, changes in response to a temperature (T) or a concentration (C) variation is what, typically, describes the sensitivity. Its relative value is expressed following equations (1) [25].

$$S_{rel} = \frac{1}{\lambda}\frac{d\lambda}{dT} \qquad S_{rel} = \frac{1}{\lambda}\frac{d\lambda}{dC}, \tag{1}$$

3.4 Whispering Gallery Modes

Whispering Gallery Modes (WGMs) are a result of optical resonance phenomena in certain cavities, generally small and spherical, such as microspheres but also micro-bottles, micro-disks and optical fiber [12]. The resonance response applies to light as it works with sound and is highly related to the geometrical symmetry, size and materials. WGMs in optical cavities is a consequence of total internal reflection phenomena in the surface of the resonator [5].

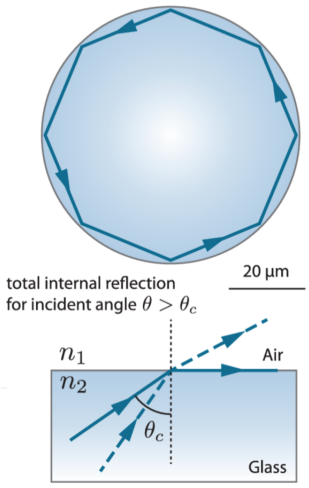

Figure 1: Optical whispering gallery [5]

For total internal reflection to occur the refractive index of the external medium has to be smaller than the refractive index of the resonator [26]. If the angle of incidence of the light is greater than the critical angle, $\theta_i > \theta_c$, total internal reflection happens, being the critical angle defined by:

$$\theta_c = sin^{-1}\left(\frac{n_a}{n_s}\right), \tag{2}$$

where n_a is the external refractive index and n_s is the index of the resonator, see Figure 1. Successive sequential internal reflections produce WGM resonances if they arrive at the starting point in-phase [12], leading to the following condition for a microsphere of radius R.

$$2\pi R n_s = l\lambda \tag{3}$$

where l is called the polar mode number and refers to the number of wavelengths that fit into the circumference. For a small value of the radius, l will also be small.

WGM resonances are described by the resonance frequency, the full width at half maximum (FWHM) and the amplitude [5]. These resonances are sensitive to changes in their external medium like a variation on the refractive index, as it will be studied in this work.

There are several researches being conducted regarding WGM in different kinds of microspheres like those made of glass, tellurite [27] and silica [23]. As pointed out in the introduction, this project is focused on resonance in glass microspheres.

3.5 Optical modes of dielectric spheres

To obtain the modes of a dielectric sphere, the Helmholtz equation, with boundary conditions, in spherical coordinates given by equation (4) has to be solved.

$$\frac{1}{r^2}\frac{\partial^2}{\partial r^2}(r\psi) + \frac{1}{r\sin(\theta)}\frac{\partial}{\partial r}\left(\sin(\theta)\frac{\partial}{\partial\theta}\psi\right) + \frac{1}{r^2\sin^2(\theta)}\frac{\partial^2}{\partial\phi^2}\psi - n^2k^2\psi = 0 \tag{4}$$

Polarization can be considered constant along the optical paths for a sphere where the modes reflect with grazing incidence upon the boundary and if the sphere is considered an homogeneous dielectric.

Helmholtz equation has two solutions, electric (TM) and magnetic (TE) in character. The field can be described with two components E_ϕ and H_ϕ. This components can be estimated by separation of variables, $\psi(\phi,\theta,r) = \psi_\phi\psi_\theta\psi_r$. TE modes have an electric field parallel to the surface while TM modes have a magnetic field parallel to the sphere's surface. The eigenfunctions can be associated with the radial mode number (n), the polar mode number (l) and the azimuthal mode number (m).

The azimuthal eigenfunctions are given by:

$$\psi_\phi = \frac{1}{\sqrt{2\pi}}\exp(\pm im\phi) \tag{5}$$

Separation of variables leads to the introduction of the azimuthal and angular mode numbers.

$$\frac{1}{\psi_\phi}\frac{d^2}{d\phi^2}\psi_\phi = \text{ const } \equiv -m^2 \qquad\qquad \frac{r}{\psi_r}\frac{d^2}{dr^2}(r\psi_r) = \text{ const } \equiv \ell(\ell+1) \tag{6}$$

Introducing the polar number ℓ, ψ_θ is given by:

$$\frac{1}{\cos(\theta)}\frac{d}{d\theta}\left(\cos(\theta)\frac{d}{d\theta}\psi_\theta\right) - \frac{m^2}{\cos(\theta)^2}\psi_\theta + \ell(\ell+1)\psi_\theta = 0 \tag{7}$$

And for the radial field, ψ_r obeys:

$$\frac{d^2}{dr^2}\psi_r + \frac{2}{r}\frac{d}{dr}\psi_r + \left(k^2 n(r)^2 - \frac{\ell(\ell+1)}{r^2}\right)\psi_r = 0 \tag{8}$$

The solutions of equations(7) and (8) can be written in terms of Legendre Polynomials ($P_m^\ell(\cos\theta)$) and the Bessel functions ($j_l(kr)$).

The field distribution and resonance locations are determined by matching the solutions inside the sphere and in the external media at the boundary, this involves the Bessel functions $j_l(kr)$ and the Hankel functions $h_l(ka)$, leading to the characteristic equation (9) [28].

$$x \cdot \frac{j_l'(kr)}{j_l(ka)} = \frac{h_l'(kr)}{h_l(kr)} \tag{9}$$

where $x = n$ for TE and $x = 1/n$ for TM.

3.6 Mie scattering and WGM

One way to study of WGMs is through Mie Scattering. When a beam of electromagnetic radiation illuminates a particle in a non-absorbing medium some part of the beam energy is absorbed and certain amount is scattered. The geometry of the problem is shown in Figure 2.

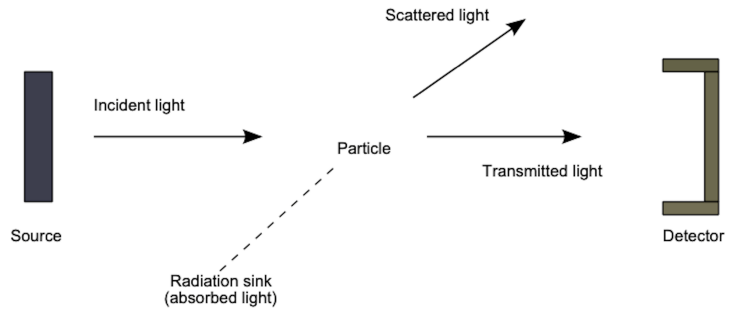

Figure 2: Scattering of a small particle [29]

The energy flow that reaches the detector is denoted by U. When there is no particle in the light path the energy that gets to the detector, would be $U_0 > U$. The particle causes some extinction of the incident beam. The difference $U_0 - U$ is due to particle absorption and scattering.

$$Extinction = Absorption + Scattering \tag{10}$$

Extinction depends on the composition of the particle, its size, shape, orientation, the composition of the surrounding medium, the number of particles if more than one was considered, the light polarization and frequency of the incident beam. Considering a single particle and an imaginary sphere of radius r around it, the energy flow that crosses the surface of the imaginary sphere (A) is given by:

$$W_a = -\int_A \vec{S} \cdot \hat{e_r} \cdot dA \tag{11}$$

where $\hat{e_r}$ refers to the scattering direction and $\vec{S}$ is the Poynting vector $\vec{S} = \vec{E} \times \vec{H}$. This energy flow can be written as the sum of three contributions $W_a = W_i - W_s + W_{ext}$:

$$W_i = -\int_A \vec{S_i} \cdot \hat{e_r} \cdot dA \qquad W_s = \int_A \vec{S_s} \cdot \hat{e_r} \cdot dA \qquad W_{ext} = -\int_A \vec{S_{ext}} \cdot \hat{e_r} \cdot dA \tag{12}$$

where $\vec{S_i}$ is the Poynting vector associated to the incident beam, $\vec{S_s}$ that of the scattered beam and $\vec{S_{ext}}$ the one related to the interaction between the incident and the scattered beam. W_i is cancelled for a transparent medium, so that W_{ext} equals to the sum $W_{ext} = W_a + W_s$

The extinction, absorption and scattering cross-sections are defined by:

$$C_{ext} = \frac{W_{ext}}{I_i} \qquad C_{sca} = \frac{W_a}{I_i} \qquad C_{abs} = \frac{W_s}{I_i} \tag{13}$$

Leading to $C_{ext} = C_{abs} + C_{sca}$.

Finally the efficiencies for extinction, absorption and scattering are defined by the expressions:

$$Q_{ext} = \frac{C_{ext}}{\mathrm{G}} \qquad Q_{sca} = \frac{C_{sca}}{\mathrm{G}} \qquad Q_{abs} = \frac{C_{abs}}{\mathrm{G}}, \tag{14}$$

where G is πa^2 for a sphere of radius r.

As a test, extinction coefficient was calculated and plotted in Figure 3 as a function of the wavelength for a water droplet, in the range $1 - 2.41\mu m$.

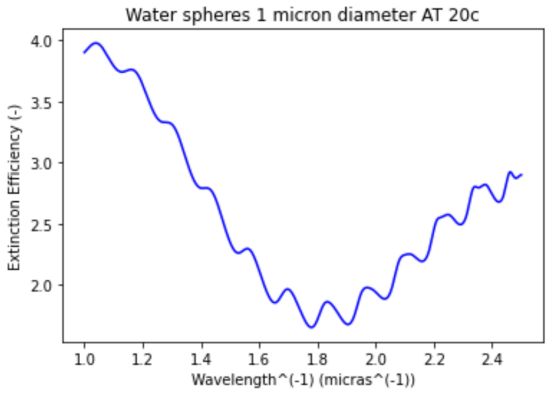

Figure 3: Extinction efficiency of water droplets in air.

and compared with the result obtained by Bohren and Huffman [30], which obtained a similar plot, in a wider range of wavelength (see Figure 4).

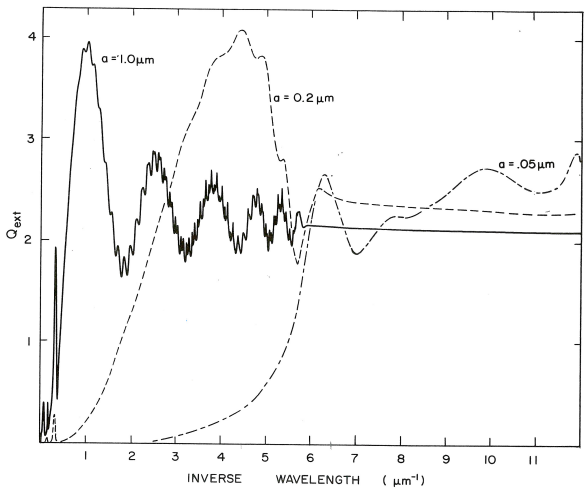

Figure 4: Extinction efficiency of water droplets in air [30]

The oscillations are interpreted as a result of the interference between the incident wave and the scattered wave. The ripple structure belongs to the resonant modes of the sphere, and those are related to the minimal values of a_n and b_n coefficients that define the extinction coefficient. a_n and b_n are the Mie coefficients; a_n are the coefficients associated with TE modes and b_n to the TM modes, given by equation (15).

$$\left.\begin{aligned} \mathbf{a}_{\mathrm{n}} &= \frac{m\psi_n(mx)\psi_n'(x)-\psi_n(x)\psi_n'(mx)}{m\psi_n(mx)\xi_n'(x)-\xi_n(x)\psi_n'(mx)} \\ \mathbf{b}_{\mathrm{n}} &= \frac{\psi_n(mx)\psi_n'(x)-m\psi_n(x)\psi_n'(mx)}{\psi_n(mx)\xi_n'(x)-m\xi_n(x)\psi_n'(mx)} \end{aligned}\right\}, \tag{15}$$

where m stands for the refractive index and ψ_n and ξ_n are the Riccati-Bessel functions.

Extinction coefficient is defined by equation (16).

$$C_{ext} = \frac{2\pi}{k^2}\sum_{n=1}^{\infty}(2n+1)Re(a_n+b_n) \tag{16}$$

Using the relation of equation (14), the extinction efficiency can be written as:

$$Q_{ext} = \frac{2\pi}{x^2}\sum_{n=1}^{\infty}(2n+1)Re(a_n+b_n), \tag{17}$$

where x is the size parameter, given by $x = kr$ [30].

If the properties of the scattering particle or the media change, a change in the C_{ext} and the ripple structure occurs. Considered a single spherical particle, the ripple structure is associated with the WGMs of the sphere. The evaluation of the extinction coefficient allows us estimate the wavelengths of the WGM of a given sphere immersed in a surrounding media, as well as to estimate the changes in wavelengths and shape of the modes produced by changes in the sphere and the media.

G. Roll et al. [31] through a geometrical optics approach gives a resonance condition for the size parameter.

$$\frac{n+1/2}{n_r} < x < n+1/2 \tag{18}$$

where n_r refers to the relative reflection index $n_r = n_{ext}/n_s$, n refers to the radial mode number and x is the size parameter.

3.6.1 Frequency displacement

The calculation of the extinction efficiency allows to numerically evaluate the displacement of the resonant modes produced by changes in the external medium, then a numerical estimation of the sensitivity of WGM can be obtained and the performance of the sensor can be analyzed. The WGM displacement is related to changes in the external medium, if the resonator is used as a temperature sensor. In this work, the sensor designed is meant to be used for temperature and concentration of a solution of glycerol in water, but the result can be applied to any change in the refractive index of the external medium regardless of how they have been produced.

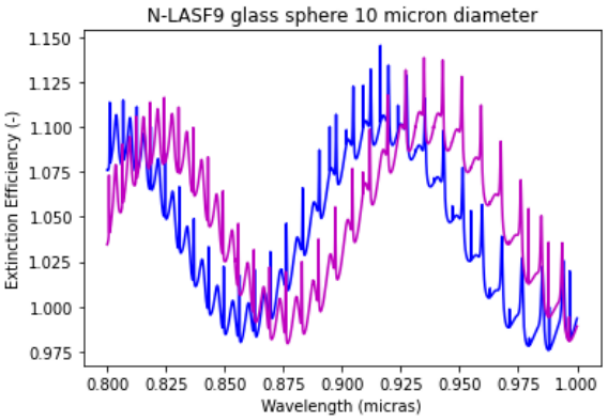

Figure 5: Extinction efficiency for LASF9 microspheres in NOA65

Figure 5 shows the shift produced in WGM for a μm LASF9 microsphere in NOA65 for a temperature change of 40^oC. As it's possible to see not only a shift takes place but also there's a change in the ripple structure.

4 Methodology

En esta sección se detalla la metodología seguida en los estudios llevados a cabo en este trabajo de fin de grado. Se describen los métodos numéricos de estimación de los modos resonantes de una esfera y a continuacion se detalla la caracterización de los medios materiales de la esfera y medios externos de interés. Finalmente se explicará como se llevará a cabo el estudio de la sensibilidad de los sensores basados en WGM.

4.1 Numerical methods for estimating resonant modes on a sphere

For modelling simulations of sensor performance, two different approaches to Whispering Gallery Modes were studied. WGM an be estimated by solving the characteristics equation for the optical modes (9) and with Mie scattering through the extinction coefficient or extinction efficiency.

4.1.1 Schiller's approximation for the solution of the characteristic equation

Resonances can be numerically predicted by Schiller algorithm, which consists in an approximation of the solution of the characteristics equation. To identify the resonances, each of them is labeled by two numbers, n and l. As mentioned in section 3.5, mode numbers n and l are related to the optical modes inside a sphere.

The resonance size parameters ${x_n}^{(l)}$ can be calculated by:

$$ {x_n}^{(l)} = \frac{\nu}{m} - \frac{\zeta_l}{m}\left(\frac{\nu}{2}\right)^{1/3} + \sum_{k=0}^{k_{\max}} \frac{d_k\left(m,\zeta_l\right)}{\nu^{k/3}\left(m^2-1\right)^{(k+1)/2}} \tag{19} $$

where ζ_l is the l'th zero of the Airy function and m is the relative refraction index $m = \frac{n_s}{n_a}$, here n_a is the index of the medium surrounding the sphere and n_s the refractive index of the sphere [32].

In (19), coefficients d_k depend on (p, m, e_k) and p values are $p = 1$ for TE modes and $p = \frac{1}{m^2}$ for TM modes. Full expressions for these parameters can be found on Appendix A.1.

The size parameter is related to the angular frequencies through the equation:

$$ \omega_n^{(l)} = {x_n}^{(l)} c/n_a R \tag{20} $$

From there the wavelength, $\lambda_n^{(l)} = \frac{2\pi c}{\omega_m^{(l)}}$, is also an approximation of the resonant wavelength for a certain n and l. As refractive index depends on wavelength, to make the approximation more accurate, a start wavelength is set and the algorithm is iterated until reaching a convergent value.

4.1.2 Bohren-Huffman algorithm

Mie scattering equations,for the extinction coefficient, introduced in section 3.6 will be used to obtain a numerical estimation of the resonance modes of a given sphere. The algorithm developed by Bohren-Huffman (B-H) calculates the scattering and extinction cross section, the extinction cross section is given by equation (21).

$$ \sigma_{ext} = \frac{2\pi}{k^2}\sum_{n=1}^{\infty}(2n+1)Re(a_n + b_n), \tag{21} $$

The coefficients a_n and b_n are given by (see also equation 15):

$$
\begin{aligned}
a_n &= \frac{m\psi_n(w)\psi_n'(v) - \psi_n(v)\psi_n'(w)}{m\psi_n(w)\xi_n'(v) - \xi_n(v)\psi_n'(w)} \\
b_n &= \frac{\psi_n(w)\psi_n'(v) - m\psi_n(v)\psi_n'(w)}{\psi_n(w)\xi_n'(v) - m\xi_n(v)\psi_n'(w)}
\end{aligned}
\tag{22}
$$

where m, v and k are defined as:

$$
\begin{aligned}
m &= n_s/n_a \\
v &= kr_0 \\
w &= mx
\end{aligned}
\tag{23}
$$

The denominators of a_n and b_n (22) have a minimum for the resonant λ; and result in a peak in the representation of the extinction coefficient, as shows Figure 6 for a sphere of radius $10\mu m$ in water.

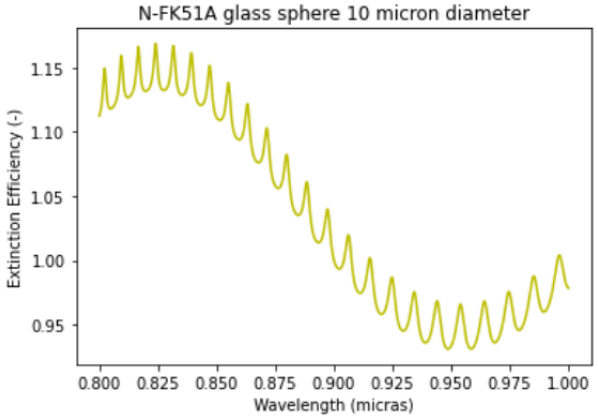

Figure 6: Extinction efficiency for a sphere of FK51A.

Identifying modes from this type of plot is one of the limitations of this method. By plotting just one coefficient, a_n or b_n, for a given set of (n, l) is more convenient. Only TE or TM modes with mode number n for different l modes if they fall in the range studied, if they fall will appear in the figure and can be easily identified.

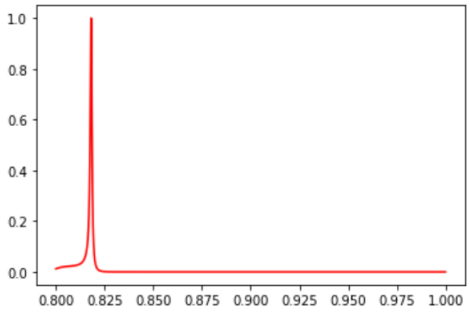

Figure 7: $a_{219,1}$ coefficient for a $20\mu m$ BAF10 sphere.

Changing any of the parameters in our equations would lead to shift of the extinction coefficient and for resonant modes as shown in figure 8 for SF10 in NOA65 for a temperature increase from 20^oC (blue) to 100^oC (red).

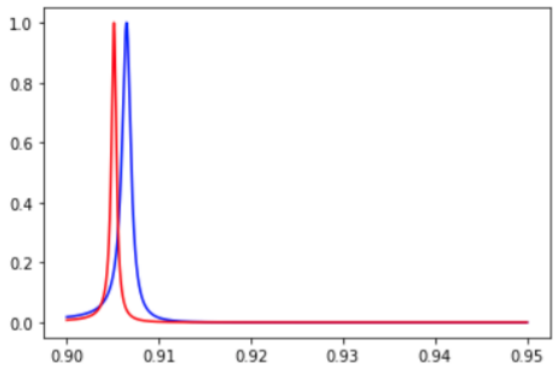

Figure 8: $a_{111,1}$ coefficient for SF10 in NOA65.

Identifying the modes is essential to pair the modes when a change in the extinction efficiency is introduced, in order to estimate the modes displacements.

4.2 Refractive index characterisation

Optical sensors design involves selecting the characteristics of an optical resonator as material used to fabricate the resonator or its size. Optical sensors based on WGM need to be characterised to test their performance, as the performance of these sensors rely on measuring frequency shifts due to refractive index variations. In this section we will talk about the properties of the materials and mediums that will be used in this work.

4.2.1 Microspheres

The refractive index of the glass changes with wavelength and temperature, so only materials that have been already characterised are going to be used.

SCHOTT has several glass types with data sheets available so expressions for the refractive index versus wavelength and temperature are available. The refractive index obeys the next equations, (24) and (25) . Several glasses from SCHOTT be used as the microsphere materials.

$$n_{abs}(\lambda, T) = n_{abs}(\lambda, T_0) + \Delta n_{abs}(\lambda, T) \tag{24}$$

$$\Delta n_{abs}(\lambda, T) = \frac{n^2(\lambda, T) - 1}{2(\lambda, T)} \cdot \left(D_0 + 2 \cdot D_1 \cdot \Delta T + 3 \cdot D_2 \cdot \Delta T^2 + \frac{E_0 + 2 \cdot E_1 \cdot \Delta T}{\lambda^2 - \lambda_{TK}^2} \right) \tag{25}$$

D_0, D_1, D_2, E_0, E_1 and λ_{TK} are constants that depend on the glass type and are given by SCHOTT data sheets [34].

The main interest of this study is detecting changes in the external medium. When the temperature changes, the size of the microsphere won't change because a glasses with low thermal expansion coefficient were chosen, and for these glasses that will be used changes in the glass refractive index with temperature increase are smaller than the changes being measured.

4.2.2 External medium

One of the external mediums that will be used is the optical glue Norland Optical Adhesive 65 (NOA65), a clear liquid photopolymer that cures under ultraviolet light (UV) [35], for which

the refractive index versus wavelength and temperature is known [36].

The other external medium that will be used is a solution of glycerine in water with different values of the concentration. The refractive index of water changes with wavelength and temperature following the expression (26) [37].

$$n(\lambda, T) = A(T) + \frac{B(T)}{\lambda^2} + \frac{C(T)}{\lambda^4} + \frac{D(T)}{\lambda^6} \tag{26}$$

A, B, C, D values are detailed in the Appendix A.2.

For glycerine the refractive index with wavelength changes as follows [38].

$$n(\lambda) = 1.45797 + 0.00598\lambda^{-2} - 0.00036\lambda^{-4} \tag{27}$$

The index of a solution of glycerine in water versus the concentration is given by:

$$n(\lambda, C) = n_{gly}(\lambda) \cdot C + n_{wat}(\lambda, T) \cdot \frac{(100 - C)}{100} \tag{28}$$

A variation in the concentration of glycerine will not affect the sphere and so the displacements of the modes will only be produced by a change in the external medium.

4.3 Procedure

To study WGMs through simulations the procedure described in this section will be used.

Using Schiller equations, the approximated wavelength of resonances are estimated for certain n,l and a given wavelength interval. Only TM modes were studied because Schiller's approximation gives more accurate results than for the TE modes. Once the resonances are approximately known in that interval the extinction efficiency and the $a_{n,l}$ coefficient are calculated with B-H algorithm. From $a_{n,l}$ data, all the TM modes with that n value and different l can be obtained and compared with the peaks of extinction coefficient and the Schiller's approximation.

The procedure is repeated for a given sphere varying the external medium index through a change of temperature or concentration of glycerine in a water solution.

As the modes are perfectly labeled the displacements in the resonance wavelength can be estimated, and so the sensitivity of the sensor to the refractive index changes.

In the next section the specific conditions and results of the simulations will be presented and analyzed.

5 Results and discussion

En esta sección se detallan las simulaciones realizadas con el objetivo de determinar que rangos de indices de refracción y tamaños de la esfera dan un desplazamiento óptimo. Una vez determinados dichos rangos se realiza un estudio de la sensibilidad. Finalmente se realiza un estudio a partir de representaciones gráficas con la finalidad de comprender el comportamiento de los WGM frente a cambios en el índice de refracción.

5.1 Resonant modes response to refractive index configurations

For this first study Norland Optical Adhesive 65 (NOA65) was used as external medium, it has a refractive index of $n \approx 1.52$ for the d line of the helium spectrum. Using different SCHOTT glasses (LASF9, SF11, SF10, SF5, BAF10 and BAK1) with refractive indexes ranging from 1.83 to 1.56 values and increasing the values of temperature from 20^oC to 30^oC, a study of resonances behavior was made following the procedure explained in section 4.3.

The study is centered in TM modes and a 10 μm microsphere, because smaller spheres support less WGM and this simplifies the study. Moreover, the results are valid for bigger sphere radius. Also azimuthal direction of the field is fixed to $l = 1$ because resonant modes with small l sharper.

The objective of the first study was to perform a rough analysis of the behaviour of the modes with the refractive index which can be used to design the following studies. This first study was done for mode $n = 105$,$l = 1$ immersing different microspheres in some external media, NOA65, and varying the temperature for each sphere. A range of wavelengths of interest is chosen based on the intervals frequently used in spectroscopy.

The results for thus numerical study are presented in Table 1.

Material	T [ºC]	n_s	n_l	λ_{Sch} [nm]	λ_{BH} [nm]	$\Delta\lambda_{Sch}$ [nm]	$\Delta\lambda_{BH}$ [nm]	Δn
LASF9	20	1.82418124	1.51688784	1014.675111	1014.761476			0.3072934028
LASF9	30	1.82419671	1.51517244	1014.607058	1014.701470	-0.0680532	-0.060006	0.3090242725
N-SF11	20	1.75655081	1.51729246	980.1134609	980.4300430			0.2392583519
N-SF11	30	1.75651234	1.51557551	979.9819616	980.4300430	-0.1314993	-0.1440144	0.2409368307
N-SF10	20	1.70514676	1.51761349	955.0713566	955.6995700			0.1875332762
N-SF10	30	1.70509685	1.51589561	954.8751651	955.4995500	-0.1961915	-0.2000200	0.1892012399
N-SF5	20	1.65401822	1.51791925	932.9210446	932.0532053			0.1360989662
N-SF5	30	1.65404009	1.51620165	932.5905747	931.8831883	-0.3304699	-0.1700170	0.1378384401
BAF10	20	1.65651496	1.51790560	933.8769330	933.2193219			0.1386093594
BAF10	30	1.65658844	1.51618758	933.5808991	933.0813081	-0.2960340	-0.1380138	0.1404008558
BAK1	20	1.56166427	1.51701204	1003.679666				0.0446522320
BAK1	30	1.56188339	1.51546523	989.1014675		-0.145782		0.0464181581

Table 1: Data table for a variation in temperature of 10^oC for different glass microspheres immersed in NOA65, for the mode with $n = 105$ $l = 1$. Blank spaces are due to errors in the Bohren-Huffman code, related to a break in the resonance condition.

Different displacements and $\Delta n = n_{sph} - n_{ext}$ values were obtained for the same temperature variation ΔT. It can be observed that $\Delta\lambda$ increases as Δn decreases until Δn reaches a value around 0.189, then an anomalous behavior in $\Delta\lambda$, that starts to decrease is produced.

To analyze the behaviour of the modes several plots are presented in Figures 9, 10 and 11.

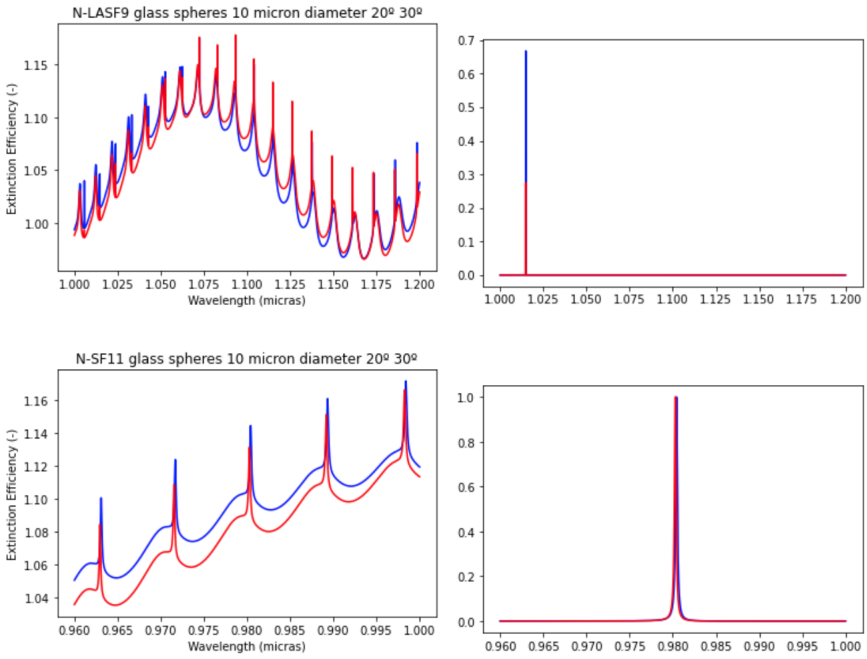

Figure 9: Extinction efficiency of a $10\mu m$ LASF0 and SF11 microspheres immersed in NOA65 for a temperature increase from 20^oC(blue) to 30^oC (red) and $a_{105,1}$ Mie coefficient.

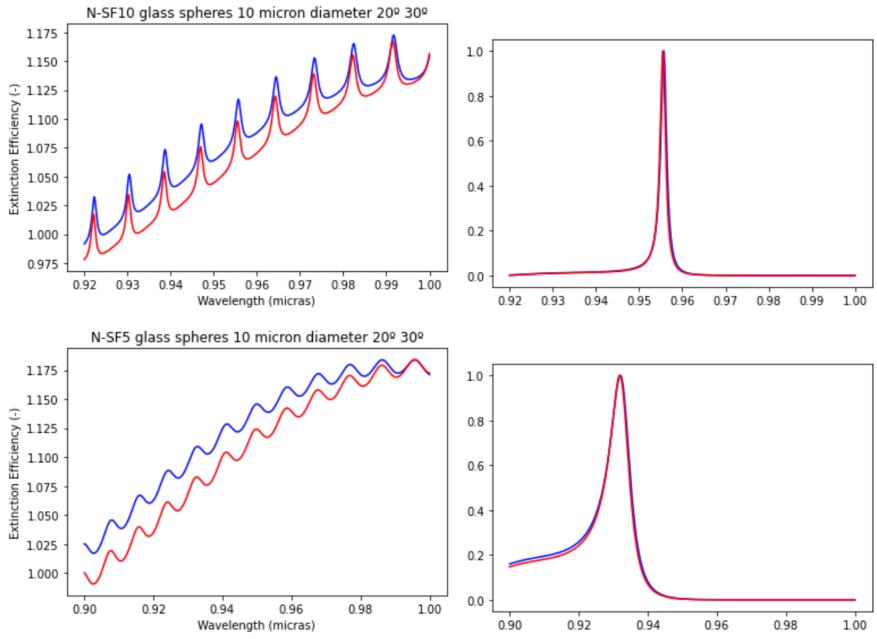

Figure 10: Extinction efficiency of a $10\mu m$ SF10 and SF5 microspheres immersed in NOA65 for a temperature increase from 20^oC (blue) to 30^oC (red) and $a_{105,1}$ Mie coefficient.

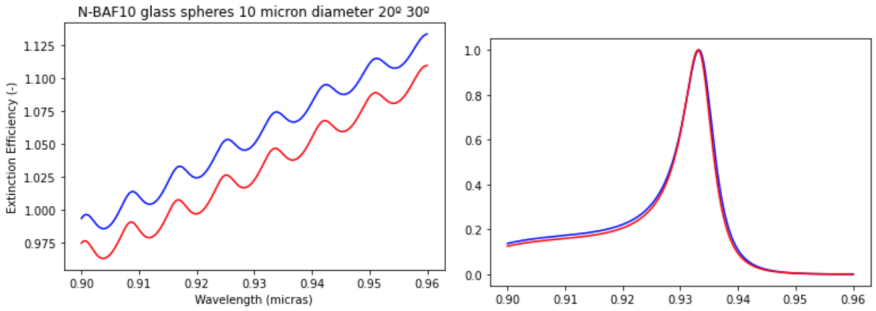

Figure 11: Extinction efficiency of a $10\mu m$ BAF10 microsphere immersed in NOA65 for a temperature increase from 20^oC (blue) to 30^oC (red) and $a_{105,1}$ Mie coefficient.

It can be seen that the smaller Δn gets, the wider the modes become. Going back to the resonance condition of equation (18), the size parameter has upper and lower bound for the resonant modes. We will calculate the size parameter for two spheres:

For NSF10 at 30^oC the resonant wavelength is $\lambda = 955.4995500$ and the refractive index value for the optical glue $n_{ext} = 1.51584561$, the size parameter given by equation (20) is $x = 99.6882$, and the upper bound of the resonance condition is $n + 1/2 = 105.5$, verifying that $99.6882 < 105.5$, and so fulfilling the condition.

For NSF5 at 30^oC the resonant wavelength is $\lambda = 931.8831883$ and the refractive index value for the optical glue $n_{ext} = 1.51620165$, the size parameter is $x = 105.217$, and as the mode under study is the same the upper bound of the resonance condition is 105.5, $105.217 < 105.5$ fulfilling the resonance condition. Although the condition is fulfilled, the values are very close.

To test this behaviour, a second study was done using an FK51A sphere immersed in a glycerine-water solution for different glycerine concentrations. The mode here analysed has $n = 106$ and $l = 1$. The results are presented in Table 2.

Concentration [%]	λ_{Sch} [nm]	λ_{BH} [nm]	n_s	n_l	$\Delta\lambda_{Sch}$ [nm]	$\Delta\lambda_{BH}$ [nm]	Δn	x
0	823.47792458	824.00240024	1.4820040326	1.3279370577			0.1540669749	101.2578921
10	825.16853271	825.51255126	1.4819823735	1.3417177652	1.6906081345	1.5101510151	0.1402646083	102.1215406
20	827.32142021	827.00270027	1.4819549257	1.3554905991	3.8434956384	3.0003000300	0.1264643266	102.9839275
30	830.15500000	828.28282828	1.4819190254	1.3692519572	6.6770754268	4.2804280428	0.1126670682	103.8686725
40	834.10837117	829.05290529	1.4818693594	1.3829947440	10.630446595	5.0505050505	0.0988746154	104.8137242
50	840.09024323	828.72287229	1.4817951219	1.3967045856	16.612318658	4.7204720472	0.0850905363	105.894914

Table 2: Data table for a FK51A microsphere immersed in a glycerine-water solution with an increase concentration on glycerine for the mode with $n = 106$ and $l = 1$.

When the glycerol concentration increases, refractive index of the solution gets closer to the sphere's index so Δn becomes smaller. It can be seen in the table that for a concentration of 50%, the size parameter is already too close to $n + 1/2$ and again an anomalous behaviour of the displacements occurs.

Figure 12 shows the plots of the modes behaviour for this second study.

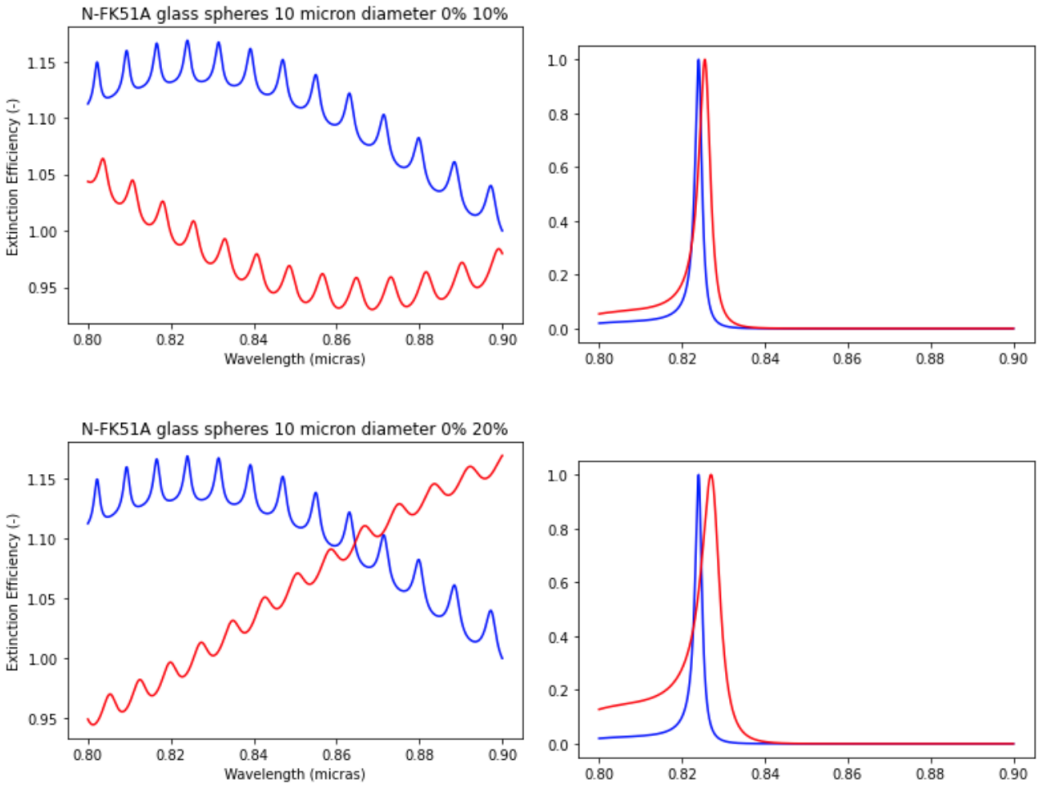

Figure 12: Extinction efficiency of FK51A microsphere in a glycerol in water solution with a concentration of 0% (blue) and concentrations of 10%, 20% (red) and a_{106} Mie coefficient.

As it can be seen in Figure 12, from a concentration of 20% modes get wider every time so peak position is not determined with enough precision, also if we analyse the rest of the study in Appendix C.1, the extinction efficiency starts to loose the ripple structure for decreasing values on the refractive index difference.

Several studies performed on the variance of the centroid algorithms, showed that the variance increases for increasing values of the peak width. Furthermore, as the modes get wider, overlapping of modes of different n and l can be produced [39] [40].

The study was repeated for BAF10 and LASF9 microspheres covering Δn values from 0.5 to 0.19 approximately. The results are shown if the Tables 3 and 4.

Concentration [%]	λ_{Sch} [nm]	λ_{BH} [nm]	n_s	n_l	$\Delta\lambda_{Sch}$ [nm]	$\Delta\lambda_{BH}$ [nm]	Δn	x
0	911.38820144	911.47014701	1.6570220275	1.3267334514			0.3302885760	91.45787337
10	911.90422929	911.941194119	1.6570101076	1.3405184850	0.0516027856	0.4710471047	0.3164916226	92.3604077
20	912.40195861	912.44824482	1.6569986235	1.3543036249	0.1013757174	0.9780978098	0.3026949986	93.258335751
30	912.93997660	913.00330033	1.6569862243	1.3680881414	0.1551775165	1.5331533153	0.2888980830	94.1568069
40	913.52444185	913.60936094	1.6569727717	1.3818719440	0.2136240417	2.1392139214	0.2751008277	95.03577641
50	914.16297621	914.28142814	1.6569580947	1.3956549216	0.2774774773	2.81128112811	0.2613031731	95.91.31207
60	914.86514745	915.03150315	1.6569419793	1.4094369356	0.3476946017	3.5613561356	0.2475050437	96.78085852
70	915.64316065	915.87758776	1.6569241528	1.4232178098	0.4254959211	4.4074407440	0.2337063429	97.63686055
80	916.51287220	916.83768377	1.6569042617	1.4369973173	0.5124670764	5.3675367537	0.2199069445	98.47894115
90	917.49531781	917.92979298	1.6568818387	1.4507751584	0.6107116373	6.4596459646	0.2061066803	99.30486219
100	918.61908593	919.16291629	1.6568562500	1.4645509290	0.7230884492	7.6927692769	0.1923053211	100.1133174

Table 3: Data table for the wavelength shifts versus concentration of a glycerin solution in water and BAF10 microsphere. The mode under study has $n = 106$ $l = 1$.

It can be seen that $\Delta\lambda$ increases as Δn decreases, and no anomalous behaviour is observed in this range due to the proper selection of the refractive index of the microsphere, that set a range of Δn bellow the critical value around 0.2. Higher values of $\Delta\lambda$ were obtained for the BAF10 microsphere due to the lower values of Δn, showing that lower values of Δn are preferred to obtain higher sensitivity, but the mode's width can not increase too much due to an increase of the centroid variance an a possible mode overlapping.

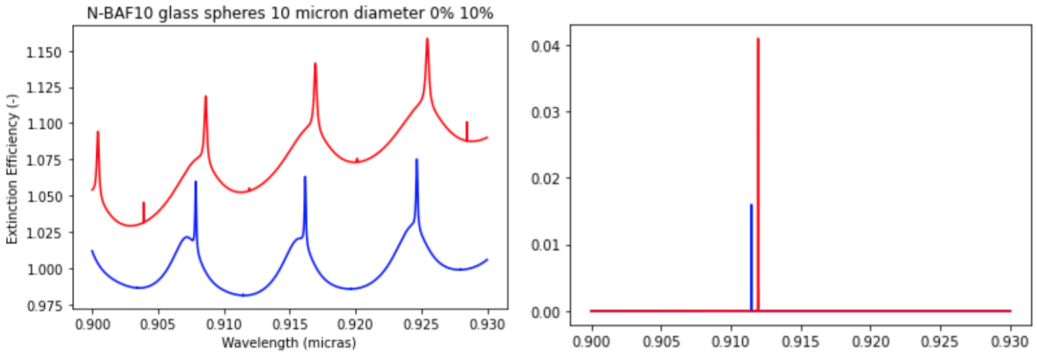

((a)) Microsphere immersed in water (blue) and in a 10% glycerin-water solution (red)

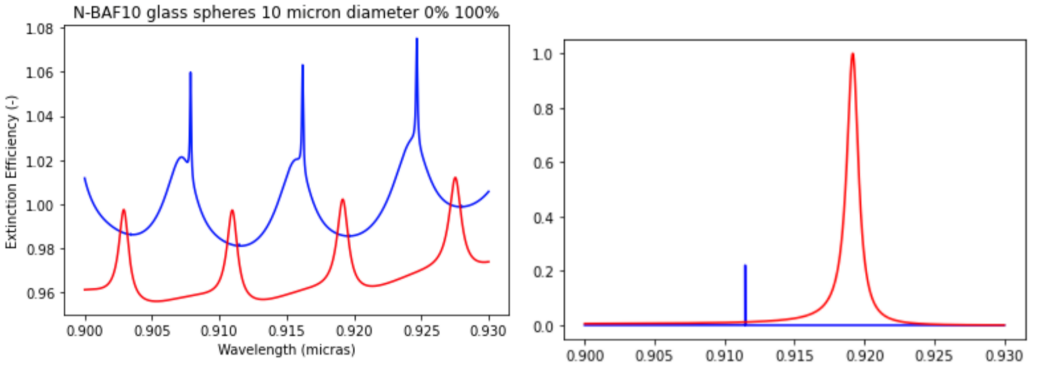

((b)) Microsphere immersed in water (blue) and in glycerine (red).

Figure 13: Plot for extinction efficiency and $a_{106,1}$ coefficient for a $10\mu m$ BAF10 microsphere.

It can be observed in Figure 13, that although the modes widen with concentration, a sharp peak is still present.

Concentration [%]	λ_{Sch} [nm]	λ_{BH} [nm]	n_s	n_l	$\Delta\lambda_{Sch}$ [nm]	$\Delta\lambda_{BH}$ [nm]	Δn	x
0	1000.0875783	1000.21162116	1.8246105515	1.3257561336			0.4988544179	83.28209034
10	1000.4794668	1000.48564856	1.8245988379	1.3395355289	0.391888504	0.2740274027	0.4850633090	84.12464449
20	1000.7649540	1000.77207720	1.8245903110	1.3533159429	0.6773757328	0.5604560456	0.4712743681	84.96574837
30	1001.0640243	1001.07250725	1.8245813842	1.3670961868	0.9764460291	0.8608860886	0.4574851974	85.80516009
40	1001.3778123	1001.38773877	1.8245720244	1.3808762470	1.2902340528	1.1761176118	0.4436957774	86.64277592
50	1001.7075994	1001.71937194	1.8245621944	1.3946561083	1.6200211844	1.5077507751	0.4299060861	87.47841974
60	1002.0548396	1002.06900690	1.8245518519	1.4084357535	1.9672613412	1.8573857386	0.4161160984	88.31191037
70	1002.4211909	1002.43824382	1.8245409488	1.4222151629	2.3336126238	2.2266226623	0.4023257860	89.14306163
80	1002.8085547	1002.82948295	1.8245294300	1.4359943141	2.7209764202	2.6178617862	0.3885351158	89.97161062
90	1003.2191244	1003.24472447	1.8245172317	1.4497731816	3.1315461416	3.0331033103	0.3747440501	90.797323324
100	1003.6554468	1003.68716872	1.8245042805	1.4635517355	3.567868527	3.4755475548	0.3609525450	91.61984976

Table 4: Data table for the variation in concentration of glycerin on water for LASF9 microspheres. For the mode with $n = 106$ $l = 1$

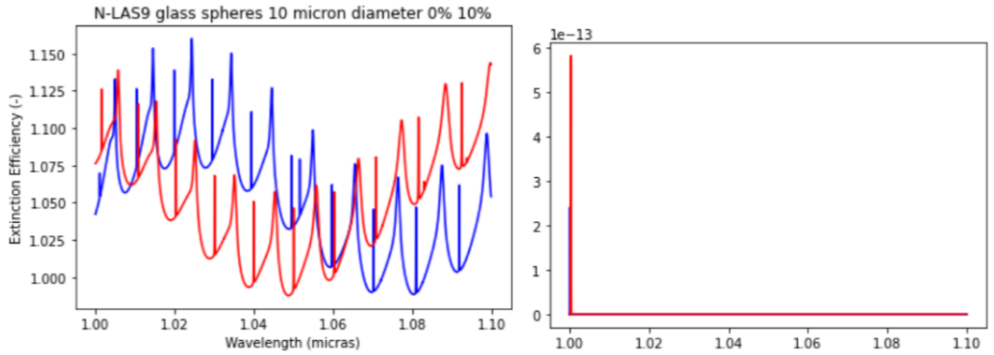

((a)) Microsphere immersed in water (blue) and in a 10% glycerin-water solution (red)

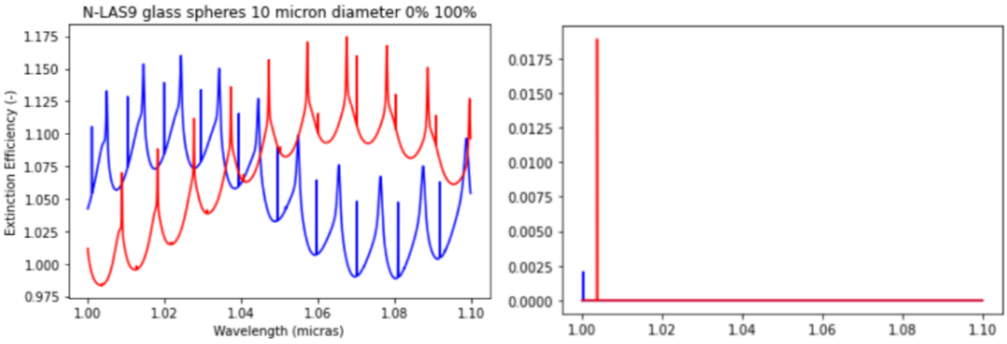

((b)) Microsphere immersed in water (blue) and in glycerine (red).

Figure 14: Plot for extinction efficiency and $a_{106,1}$ coefficient for a $10\mu m$ LASF9 microsphere.

Figure 14 shows sharp modes for LASF9 for all the glycerine concentrations in water because Δn values are not as small as the BAF10 values so there's no breaking of the resonance condition and the wavelength shift is smaller, as expected.

5.2 Microsphere size

In this section we will present a short study of the WGM displacement versus the microsphere size. Two microspheres of BAF10 and radius of $10\mu m$ and $20\mu m$, immersed first in water ans secondly in a solution of 40% of glycerine in water were used. The behaviour of the mode with $n = 106$ and $l = 1$ was studied an the results are shown in Table 5.

n *mode*	R $[\mu m]$	*Concentration* [%]	λ_{Sch} [nm]	x_{Sch} [nm]	λ_{BH} [nm]	x_{BH} [nm]	n_s	n_l	$\Delta\lambda_{Sch}$ [nm]	$\Delta\lambda_{BH}$ [nm]	Δn
106	10	0	911.44175	91.46068	911.46723	91.4579	1.65702	1.32673			0.33029
106	10	40	913.52444	95.04461	913.61027	95.03561	1.65697	1.38197	2.08269	2.14104	0.2751
106	20	0	1808.19854	91.86766	180.82562	91.86472	1.6433	1.32190			0.3214
106	20	40	1812.51061	95.47182	181.27063	95.46149	1.64324	1.37704	4.31207	4.45008	0.2662
218	20	0	910.66958	183.07776	910.66066	182.63742	1.65704	1.32674			0.3303
218	20	40	911.57422	190.49932	911.56156	190.37834	1.65702	1.3819	0.90464	0.90090	0.27512

Table 5: Data table for size dependence, variation on concentration of glycerine on water for BAF10 microspheres for $l = 1$

It can be seen that with a $20\mu m$ sphere the displacement increases in a factor around 2, but the wavelength of the resonance also shifts and may lay outside interval of interest. For the $r = 20\mu m$ sphere, a mode laying in the same wavelength range as the mode with $n = 106$ and $l = 1$ was studied; obtaining a displacement lower than the one obtained with the smaller sphere. It can be concluded that, if the interval of wavelengths is unchanged bigger spheres do not produce higher sensitivity.

5.3 Sensitivity study

A sensitivity study can be done through the analysis of the slope of the plots $\Delta\lambda$ versus ΔC or $\Delta\lambda$ versus ΔT.

5.3.1 Concentration

With the previous data for LASF10 (Table 4) and BAF10 (Table 3), which fulfilled the resonance condition a plot of displacement versus glycerol concentration was performed.

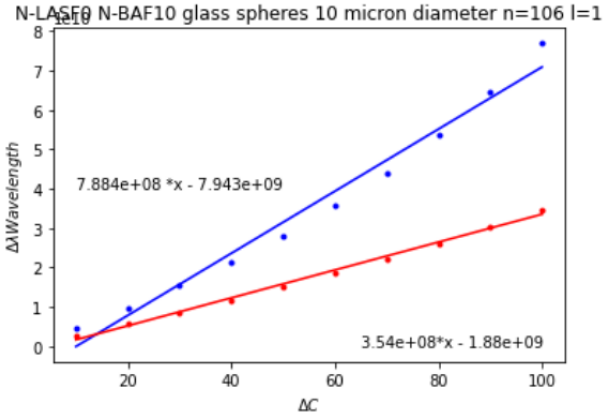

Figure 15: $\Delta\lambda$ versus ΔC for BAF10 (blue) and LASF9 (red) for a concentration of glycerine in water ranging from 0% to 100%.

If we define the sensitivity as the rate of change of the wavelength with concentration, the sensitivities obtained for LASF0 and BAF10 are $S_{LASF9} = 3.54 \cdot 10^8$ and $S_{BAF10} = 7.884 \cdot 10^8$, concluding that lower values of Δn are associated to higher values of sensitivity, and this parameter is a key factor in the design of an optical WGM sensor.

5.3.2 Temperature

A study with temperature was performed for SF10 and LASF9 in NOA56 and the mode with $n = 111$ and $l = 1$. Tables 6 and 7 can be found in Appendix B, with the data belonging to this study. The resonance condition is fulfilled in all the temperature range for both microspheres.

For the SF10 microsphere the experiment was repeated for another mode, $n = 118$ and as expected the resonator's behaviour didn't change. A data table is included on Appendix B, table 8.

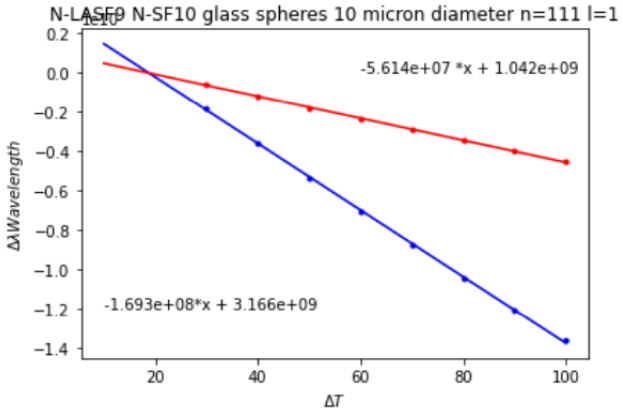

Figure 16: $\Delta\lambda$ versus ΔT for SF10 (blue) and LASF9 (red) in NOA65 for a temperature increase from 20^{o} to 100^{o}.

The slope has a negative value because for increasing values of the temperature, the wavelength shifts to lower values.Taking the absolute values, the sensitivities obtained are $S_{LASF9} = 5.614 \cdot 10^7$ and $S_{SF10} = 1.693 \cdot 10^8$. Again, higher sensitivities are associated to lower values of Δn.

5.4 Analysis of the ripple structure

With the aim of understanding the behaviour of the WGM under changes in the refractive index difference, a plot of the extinction efficiency and $a_{n,l}$ for a SF10 microsphere in water and in glycerine are presented. Modes with $l = 2$ are also shown in the plots. Selecting one of the glasses more suitable for a concentration study of glycerol in water, SF10.

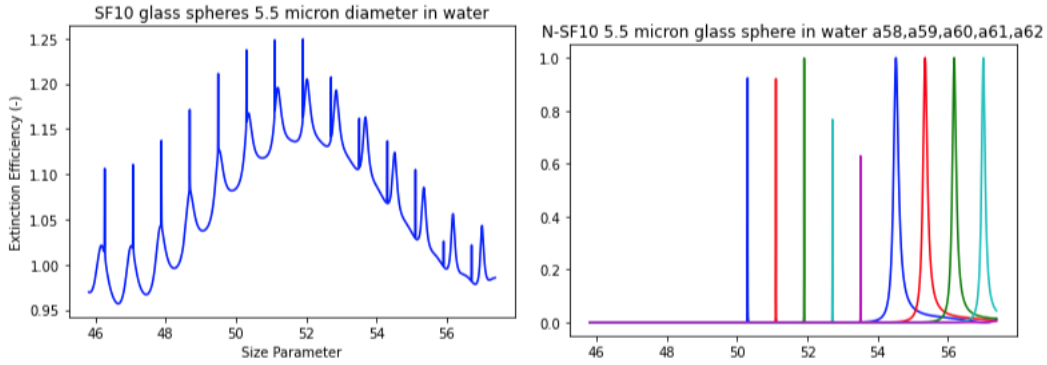

Figure 17: Whispering gallery modes and plot for several Mie coefficients for a SF10 microsphere of $5.5\mu m$ in water versus size parameter.

Figure 17 shows the results for the microsphere immersed in water. The left plot shows the extinction coefficient versus size parameter and the rigth plot the modes modes a_{58}(blue), a_{59}(red), a_{50} (green),a_{61} (cyan) and a_{62} (magenta).

Modes with $l = 1$ and $l = 2$ are shown in the plot. It can be seen that modes with $l = 2$ are wider than modes with $l = 1$.

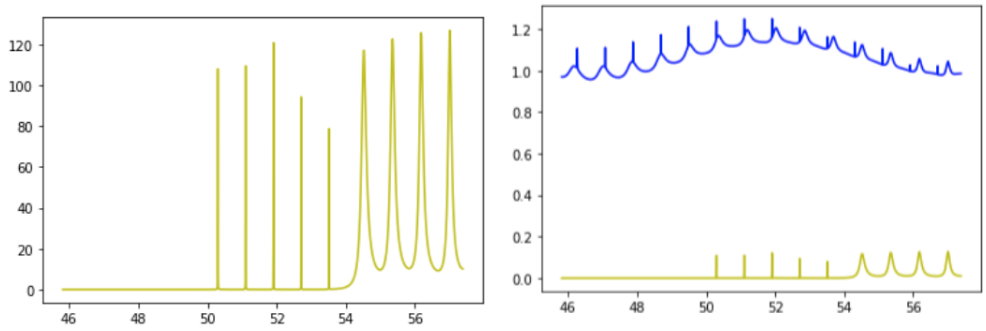

((a)) Sum of some Mie coefficients

((b)) Sum of several Mie coefficients (yellow) and WGMs (blue)

Figure 18: SF10 5.5μm microspheres immersed in water.

Figure 18 shows (a) the sum of the coefficients a_{58} to a_{62} shown in Figure 17 and (b) the sum plotted simultaneously with the extinction efficiency. It can be seen that the peaks in the sum can also be identified in the extinction efficiency and does not vanish due to mode overlapping.

The results for the study of the sphere embedded in glycerol are shown in Figures 19 and 20. It can be seen that the mode width increases for both $l = 1$ and $l = 2$ and the modes with $l = 2$ do not show in the extinction efficiency nor in the sum of a_{58} to a_{62} modes due to a break in the resonance condition for the modes with $l = 2$ and mode overlapping.

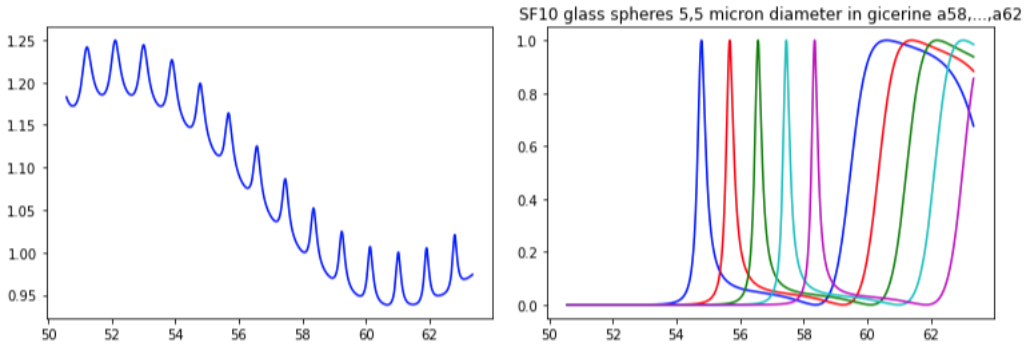

Figure 19: Whispering gallery modes and plot for several Mie coefficients for a SF10 microsphere of 5.5μm in glycerol versus size parameter.

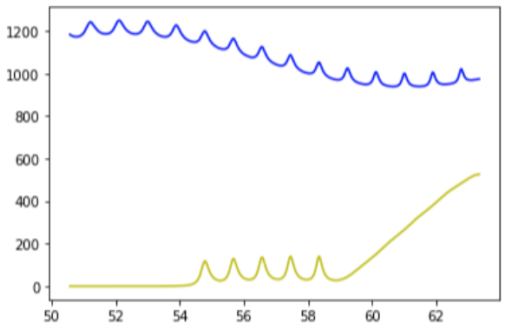

Figure 20: Sum of several Mie coefficients (yellow) and Whispering gallery modes (blue) for a SF10 microsphere in glycerine.

6 Conclusions

En esta sección se presentan las conclusiones obtenidas como resultado de este trabajo de fin de grado. En primer lugar se comentan las conclusiones asociadas al estudio de la configuración óptima de índices de refracción del sensor y del estudio con el tamaño de la microesfera.
A continuación se detallan los resultados del estudio de la sensibilidad y finalmente se habla sobre las conclusiones obtenidas del estudio de la estructura ondulante del coeficiente de extinción.

The main conclusions obtained in this work, related to the design of an optimal sensor in terms of sensitivity are listed bellow.

- A first study was made to obtain a rough estimate of the wavelength shifts versus the refractive index difference (Δn). In this first study Δn was decreased obtaining an increasing value of $\Delta\lambda$ and also an anomalous behaviour for Δn for values of Δn bellow 0.2. The mode profiles were presented in several graphs for different values of $\Delta\lambda$, showing a increase of the mode width as Δn decreased. The resonance condition for the size parameter was also evaluated, showing that the anomalous behaviour of $\Delta\lambda$ occurred for values of x too close to the upper bound of the resonance condition. This preliminary study allows to conclude that a decrease of the refractive index difference brings a higher value of the of the sensitivity but this difference can not be decreased at will.

- A second study was made selecting as an external media a solution of glycerol in water with varying concentrations and two microspheres made of LASF9 and BAF10 which produce values of Δn well bellow the critical value (0.2), obtained in the previous study, for all the range of glycerol concentrations. The WGM shifts were calculated for concentrations varying from 0% to 100% for the two spheres, and the profile of the modes here studied were plotted to observe their width variation. As a verification the resonance condition for the size parameter was also evaluated, obtaining that it was fulfilled for both spheres in all the range of Δn. This study was also done for SF10 and BAF10 immersed in NOA65 for a temperature increase from 20^oC to 1000^oC. In this study we have obtained the numerical values of the sensitivity for both spheres ($S_{LASF9} = 3.54 \cdot 10^8$ and $S_{BAF10} = 7.884 \cdot 10^8$ for the concentration increase and $S_{LASF9} = 5.614 \cdot 10^7$ and $S_{SF10} = 1.693 \cdot 10^8$ for the temperature increase) showing that lower values of Δn lead to higher values of the sensitivity and that a proper combination of the refractive index of the sphere and external medium has to be chosen to guarantee that the resonance condition is always fulfilled.

- The study for the effect of microsphere size in the shift of the WGMs showed that although the mode shift increases with the sphere radius,the wavelength range change considerably and the displaced mode can fall outside the range of interest. When only modes of different n, l but falling in the same wavelength range for two spheres of different radius were studied, it was obtained that the modes of the smaller sphere lead to a bigger displacement. This allow us to conclude that if the wavelength range is unchanged, a bigger sphere does not increase the sensitivity of the sensor.

- A final graphical study of the widths of WGM, showed that if the mode width increases the modes do not appear as peaks of the extinction efficiency due to mode overlapping associated to a break in the resonance condition.

References

[1] Xuanbin Liu, Zhuangqi Cao, Qishun Shen, and Shu Huang, "Optical sensor based on Fabry-Perot resonance modes," Appl. Opt. 42, 7137-7140 (2003)

[2] Xiuhong Liu, Chaoying Shi, Jinhua Hu, Huaying Wang, Haiyan Han, Jijun Zhao,"Improving the sensitivity of refractive index sensors with integrated double-layer resonant meta-grating structure",Optics Communications,Volume 515,2022,128171,ISSN 0030-4018,https://doi.org/10.1016/j.optcom.2022.128171.

[3] Del Villar, Ignacio & Arregui, Francisco & Zamarreño, Carlos & Corres, Jesus & Bariain, Candido & Goicoechea, Javier & Cesar, Elosua & Hernaez, Miguel & Rivero, Pedro & Socorro Leránoz, Abián & Urrutia, Aitor & Sanchez, Pedro & Zubiate, Pablo & Lopez-Torres, Diego & De Acha, Nerea & Ascorbe, Joaquin & Matias, Ignacio. (2016). "Optical sensors based on lossy-mode resonances." Sensors and Actuators B: Chemical. 240. 10.1016/j.snb.2016.08.126.

[4] Juejun Hu, Xiaochen Sun, Anu Agarwal, and Lionel C. Kimerling, "Design guidelines for optical resonator biochemical sensors," J. Opt. Soc. Am. B 26, 1032-1041 (2009)

[5] Foreman MR, Swaim JD, Vollmer F. "Whispering gallery mode sensors". Adv Opt Photonics. 2015 Jun 30;7(2):168-240. doi: 10.1364/AOP.7.000168. PMID: 26973759; PMCID: PMC4786191.

[6] Shah RY, Agrawal YK. Introduction to fiber optics: Sensors for biomedical applications. Indian J Pharm Sci. 2011 Jan;73(1):17-22. doi: 10.4103/0250-474X.89752. PMID: 22131617; PMCID: PMC3224405.

[7] Donati, S. (1988). Magneto-optical fibre sensors for electrical industry: analysis of performances. IEE Proceedings J Optoelectronics.

[8] Pedrol, Eric et al. "Optofluidic Device for the Quantification of Circulating Tumor Cells in Breast Cancer." Scientific Reports 7.1 (2017).

[9] Yin-Chu Chen, Jennifer J. Brazier, Mingdi Yan, Paulo R. Bargo, Scott A. Prahl. "Fluorescence-based optical sensor design for molecularly imprinted polymers",Sensors and Actuators B: Chemical, Volume 102, Issue 1, 2004, Pages 107-116, ISSN 0925-4005.

[10] B.D. Gupta, Anuj K. Sharma,"Sensitivity evaluation of a multi-layered surface plasmon resonance-based fiber optic sensor: a theoretical study",Sensors and Actuators B: Chemical,Volume 107, Issue 1,2005,Pages 40-46,ISSN 0925-4005.

[11] K. Wang et al., "Advances in Optical Fiber Sensors Based on Multimode Interference (MMI): A Review," in IEEE Sensors Journal, vol. 21, no. 1, pp. 132-142, 1 Jan.1, 2021, doi: 10.1109/JSEN.2020.3015086.

[12] Vollmer, F., Yu, D. (2020). "Whispering Gallery Modes in Optical Microcavities. In: Optical Whispering Gallery Modes for Biosensing." Biological and Medical Physics, Biomedical Engineering. Springer, Cham.

[13] Rho D, Breaux C, Kim S. "Label-Free Optical Resonator-Based Biosensors." Sensors (Basel). 2020 Oct 19;20(20):5901. doi: 10.3390/s20205901. PMID: 33086566; PMCID: PMC7589515.

[14] Dr. Rüdiger Paschotta, "Optical Resonators. Encyclopedia of Laser Physics and Technology" https://www.rp-photonics.com/optical_resonators.html

[15] Weidong Chen, Dean S. Venables, "3 - Broadband optical cavity methods" Spectroscopic Monitoring of the Atmosphere, Elsevier,2021,Pages 95-158.

[16] Corney, Alan, "Resonant modes of optical cavities", Atomic and Laser Spectroscopy, Oxford Classic Texts in the Physical Sciences (Oxford, 2006; online edn, Oxford Academic, 1 Sept. 2007),

[17] Alnshtein, L. A. V. (1963). "Open resonators for lasers." Soviet Physics JETP, 17(3).

[18] Evgeni A. Bezus, Dmitry A. Bykov, and Leonid L. Doskolovich, "Integrated Gires–Tournois interferometers based on evanescently coupled ridge resonators," Opt. Lett. 45, 5065-5068 (2020)

[19] Jennifer A. Black, Grant Brodnik, Haixin Liu, Su-Peng Yu, David R. Carlson, Jizhao Zang, Travis C. Briles, and Scott B. Papp, "Optical-parametric oscillation in photonic-crystal ring resonators", Optica 9, 1183-1189 (2022)

[20] Riesen N, Reynolds T, François A, Henderson MR, Monro TM. " Q-factor limits for far-field detection of whispering gallery modes in active microspheres." Opt Express. 2015 Nov 2;23(22):28896-904. doi: 10.1364/OE.23.028896. PMID: 26561158.

[21] Matthew R. Foreman, Jon D. Swaim, and Frank Vollmer, "Whispering gallery mode sensors," Adv. Opt. Photon. 7, 168-240 (2015)

[22] Von Klitzing, Wolf & Long, Romain & Ilchenko, Vladimir & Hare, Jean & Lefèvre-Seguin, Valérie. (2001). "Frequency tuning of the whispering-gallery modes of silica microspheres for cavity quantum electrodynamics and spectroscopy." Optics Letters. 26. 166-168. 10.1364/OL.26.000166.

[23] Yosuke Minowa, Yusuke Toyota, Masaaki Ashida. "In-situ tuning of whispering gallery modes of levitated silica microspheres" https://arxiv.org/abs/1701.00106

[24] J. Pan, T.-G. Cha, H. Chen, J.H. Choi, "10 - Carbon nanotube-based optical platforms for biomolecular detection" Editor(s): Shinji Yamashita, Yahachi Saito, Jong Hyun Choi, In Woodhead Publishing Series in Electronic and Optical Materials,Carbon Nanotubes and Graphene for Photonic Applications, Woodhead Publishing,2013.

[25] Martin, Leopoldo Perez-Rodriguez, Carla Haro-González, Patricia Martin I. "Whispering gallery modes in a glass microsphere as a function of temperature." Optics express. 19. 25792-8. 10.1364/OE.19.025792. (2011)

[26] Dr. Rüdiger Paschotta,"Total internal reflection. Encyclopedia of Laser Physics and Technology" https://www.rp-photonics.com/total_internal_reflection.html

[27] Andrianov, A.V., Marisova, M.P., Dorofeev, V.V., Anashkina, E.A. (2020). "Thermal shift of whispering gallery modes in tellurite glass microspheres." Results in physics, 17, 103128

[28] Kippenberg, Tobias Jan August (2004) "Nonlinear Optics in Ultra-High-Q Whispering-Gallery Optical Microcavities." Dissertation (Ph.D.), California Institute of Technology. doi:10.7907/T5B6-9R14.

[29] Thøgersen, Nora Klevjer, "Use of the Resonance Structure of Mie Scattering for Refractive Index Estimation" Norwegian University of Life Sciences,Faculty of Environmental Science and Technology Department of Mathematical Sciences and Technology. 2015-07-08.

[30] Craig F. Bohren, Donald R. Huffman "Absorption and Scattering of Light by Small Particles" 23 April 1998

[31] G. Roll, T. Kaiser, and G. Schweiger, "Eigenmodes of spherical dielectric cavities: coupling of internal and external rays," J. Opt. Soc. Am. A 16, 882-895 (1999)

[32] S. Schiller. "Asymptotic expansion of morphological resonance frequencies in Mie scattering," Appl. Opt. 32, 2181-2185 (1993)

[33] SCHOTT "TIE-19: Temperature Coefficient of the Refractive Index", Technical Information Advanced Optics (July 2008)

[34] SCHOTT AG.(s.f.) SCHOTT. Glass Made of Ideas. https://www.schott.com/

[35] Norland Products https://www.norlandprod.com

[36] Li, Jun Baird, Greg Lin, Yi-Hsin Ren, Hongwen Wu, Shin-Tson. (2005). Refractive-index matching between liquid crystals and photopolymers. Journal of The Society for Information Display - J SOC INF DISP. 13. 10.1889/1.2150371.

[37] Alexey N. Bashkatov and Elina A. Genina "Water refractive index in dependence on temperature and wavelength: a simple approximation", Proc. SPIE 5068, Saratov Fall Meeting 2002: Optical Technologies in Biophysics and Medicine IV, (13 October 2003); https://doi.org/10.1117/12.518857

[38] J. Rheims, J Köser and T Wriedt." Refractive-index measurements in the near-IR using an Abbe refractometer",Meas. Sci. Technol. 8, 601-605 (1997)

[39] Sandrine Thomas, "Optimized centroid computing in a Shack-Hartmann sensor," Proc. SPIE 5490, Advancements in Adaptive Optics, (25 October 2004); https://doi.org/10.1117/12.550055

[40] Zhiling Jiang, Shunsheng Gong, Yang Dai,"Numerical study of centroid detection accuracy for Shack-Hartmann wavefront sensor",Optics & Laser Technology,Volume 38, Issue 8,2006,Pages 614-619,ISSN 0030-3992.

.

A Detailed expressions

A.1 Schiller

$$
\begin{aligned}
d_0 &= -p \\
d_1 &= 2^{1/3}3\left(m^2-1\right)\zeta_l^2/(20m) \\
d_2 &= -2^{2/3}m^2p\left(-3+2p^2\right)\zeta_l/6 \\
d_3 &= \frac{350m^4(1-p)p\left(-1+p+p^2\right)+\left(m^2-1\right)^2\left(10+\zeta_l^3\right)}{700m} \\
d_4 &= \frac{-2^{1/3}m^2\zeta_l l_l^2\left(4-m^2+e_4\right)}{20} \\
d_5 &= \frac{\zeta_l\left[40\left(-1+3m^2-3m^4+351m^6\right)-479\left(m^2-1\right)^3\zeta_l^3-e_5\right]}{2^{4/3}63{,}000m} \\
d_6 &= \frac{5m^2\left(-13-16m^2+4m^4\right)+2m^2\left(128-4m^2+m^4\right)\zeta_l^3-e_6}{1400} \\
d_7 &= \frac{\zeta_l^2\left[100\left(-551+2204m^2-3306m^4-73{,}256m^6+10{,}229m^8\right)-20{,}231\left(m^2-1\right)^4{\zeta_l}^3+e_7\right]}{2^{2/3}16{,}170{,}000m} \\
d_8 &= \frac{m^2\zeta_l\left[10\left(11{,}082+44{,}271m^2-288m^4+7060m^6\right)-3\left(52{,}544+48{,}432m^2-11{,}496m^4+2395m^6\right)\zeta_l^3\right]+e_8}{2^{10/3}141{,}750}\,[32]
\end{aligned}
\tag{29}
$$

e_k is defined as $e_k = (m^2-1)e'_k$, this coefficient equals zero for TE and expressions for TM are the following ones.

$$
\begin{aligned}
e'_4 =& \left(-8+12m^4+m^8\right)/m^8 \\
e'_5 =& 7000m^{-6}\left(-28-m^2+56m^4-16m^6-7m^8+2m^{10}\right) \\
e'_6 =& m^{-8}\left[5\left(-200-32m^2+526m^4-226m^6-99m^8+62m^{10}+4m^{12}\right)\right. \\
&\left.+2\left(-400+272m^2+744m^4-424m^6-366m^8-2m^{10}+m^{12}\right)\zeta_l^3\right] \\
e'_7 =& -269{,}500m^{-8}\left(-232+160m^2+543m^4-447m^6-186m^8+165m^{10}-15m^{12}+4m^{14}\right) \\
e'_8 =& m^{-10}\zeta_l\left[-10\left(-459{,}200+286{,}000m^2+1{,}360{,}312m^4-1{,}305{,}476m^6-433{,}952m^8+717{,}562m^{10}\right.\right. \\
&\left.-209{,}039m^{12}-21{,}542m^{14}+7060m^{16}\right)+3\left(336{,}000-441{,}600m^2-626{,}496m^4+891{,}008m^6\right. \\
&\left.\left.+306{,}416m^8-505{,}696m^{10}-72{,}488m^{12}-7664m^{14}+2395m^{16}\right)\zeta_l^3\right]\,[32]
\end{aligned}
\tag{30}
$$

A.2 Water refractive index

$$
\begin{aligned}
A(t) &= 1.3208-1.2325\cdot10^{-5}t-1.8674\cdot10^{-6}t^2+5.0233\cdot10^{-9}t^3 \\
B(t) &= 5208.2413-0.5179t-2.284\cdot10^{-2}t^2+6.9608\cdot10^{-5}t^3 \\
C(t) &= -2.55511\cdot10^{8}-18341.336t-917.2319t^2+2.7729t^3 \\
D(t) &= 9.3495+1.7855\cdot10^{-3}t+3.6733\cdot10^{-5}t^2-1.2932\cdot10^{-7}t^3[37]
\end{aligned}
\tag{31}
$$

B Data tables

T [ºC]	n_s	n_l	λ_{Sch} [nm]	λ_{BH} [nm]	$\Delta\lambda_{Sch}$ [nm]	$\Delta\lambda_{BH}$ [nm]	Δn
20	1.7068091220	1.5183221775	905.95551708	906.49564956			0.1884869445
30	1.7067612623	1.5166001415	905.78375386	906.31563156	-0.1717632	-0.1800180	0.1901611207
40	1.7067161392	1.5148780146	905.61590722	906.13561356	-0.3396099	-0.3600360	0.1918381245
50	1.7066735732	1.5131558001	905.45182294	905.96059606	-0.5036941	-0.5350535	0.1935177731
60	1.7066333850	1.5114335012	905.29134869	905.79057906	-0.6641684	-0.7050705	0.1951998838
70	1.7065953949	1.50971112111	905.13433403	905.62056206	-0.8211831	-0.8750875	0.1968842738
80	1.7065594231	1.5079886630	904.98063026	905.45054505	-0.9748868	-1.0451045	0.1985707603
90	1.7065252904	1.5062661298	904.83009041	905.29052905	-1.1254267	-1.2051205	0.2002591606
100	1.7064928166	1.5045435245	904.68256916	905.13051305	-1.2729479	-1.3651365	0.2019492921

Table 6: Data table for a variation on temperature for a $10\mu m$ SF10 microsphere and the mode with $n = 111$ and $l = 1$.

T [ºC]	n_s	n_l	λ_{Sch} [nm]	λ_{BH} [nm]	$\Delta\lambda_{Sch}$ [nm]	$\Delta\lambda_{BH}$ [nm]	Δn
20	1.8257706171	1.5175101973	962.91803438	962.98129813			0.3082604198
30	1.8257868027	1.5157911015	962.85878866	962.92129213	-0.0592457	-0.0600060	0.3099957012
40	1.8258043350	1.5140719797	962.80086136	962.86128613	-0.1171730	-0.1200120	0.3117323553
50	1.8258231245	1.5123528329	962.74419835	962.80128013	-0.1738360	-0.1800180	0.3134702916
60	1.8258430816	1.5106336621	962.68874561	962.74627463	-0.2292888	-0.2350235	0.3152094195
70	1.8258641170	1.5089144682	962.63444923	962.69126913	-0.2835851	-0.2900290	0.3169496488
80	1.8258861410	1.5071952521	962.58125544	962.63626363	-0.3367789	-0.3450345	0.3186908889
90	1.8259090643	1.5054760148	962.52911054	962.58125813	-0.3889238	-0.4000400	0.3204330494
100	1.8259327972	1.5037567572	962.47796096	962.52625263	-0.4400734	-0.4550455	0.3221760400

Table 7: Data table for a variation on temperature for $10\mu m$ LASF10 microspheres and the mode with $n = 111$ and $l = 1$.

T [ºC]	n_s	n_l	λ_{Sch} [nm]	λ_{BH} [nm]	$\Delta\lambda_{Sch}$ [nm]	$\Delta\lambda_{BH}$ [nm]	Δn
20	1.8276531055	1.5182747864	909.00627878	909.05090509			0.3093783192
30	1.8276702066	1.5165511462	908.95553032	909.00090009	-0.0507485	-0.0500050	0.31111906039
100	1.8278232743	1.5044849513	908.63121522	908.66586659	-0.3750636	-0.3850385	0.3233383230

Table 8: Data table for a variation on temperature for a $10\mu m$ SF10 microsphere and the mode with $n = 118$ and $l = 1$.

C Figures

C.1 Glycerine concentration in water

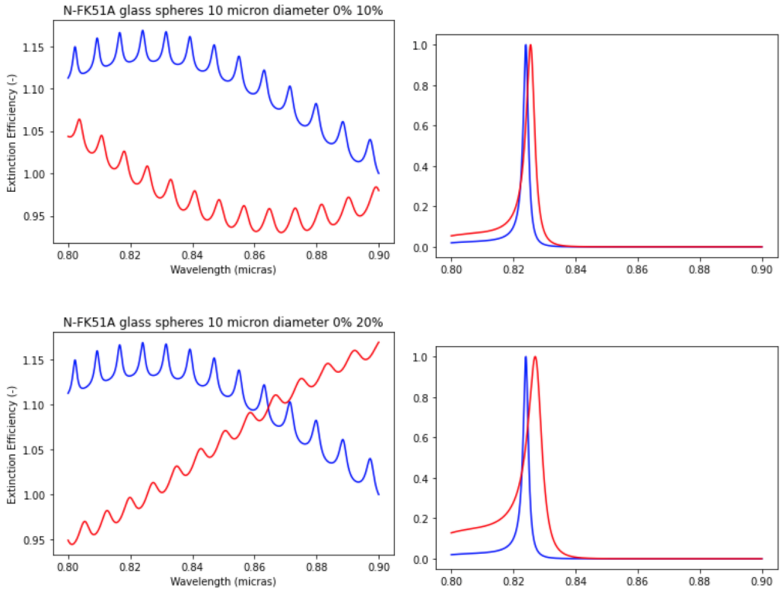

Figure 21: Plot for extinction efficiency and $a_{106,1}$ Mie coefficient for a $10\mu m$ FK51A microsphere immersed in water (blue) and a solution of glycerine in water with 10% and 20% concentrations of glycerin (red).

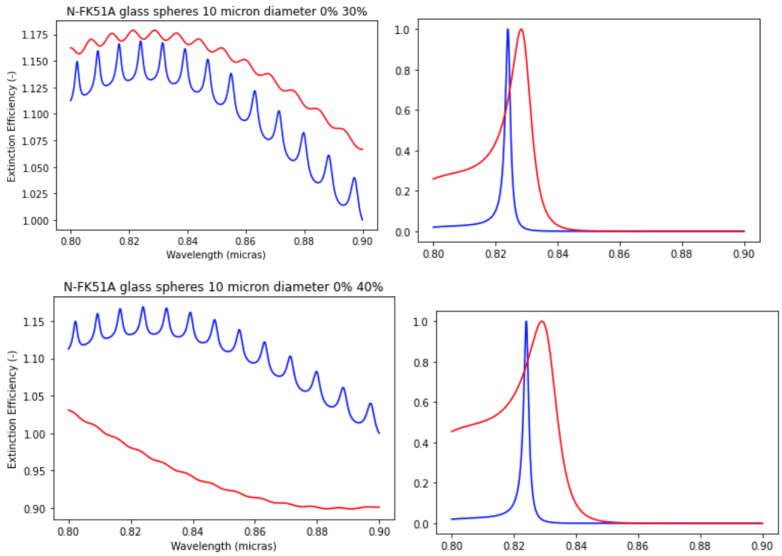

Figure 22: Plot for extinction efficiency and $a_{106,1}$ Mie coefficient for a $10\mu m$ FK51A microsphere immersed in water (blue) and a solution of glycerine in water with 30% and 40% concentrations of glycerin (red).

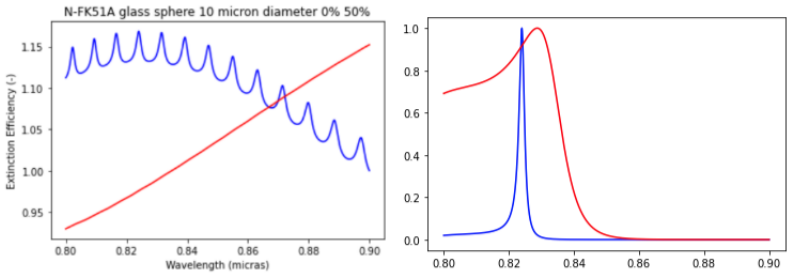

Figure 23: Plot for extinction efficiency and $a_{106,1}$ Mie coefficient for a $10\mu m$ FK51A microsphere immersed in water (blue) and a solution of glycerine in water with a 50% concentration of glycerin (red).

C.2 Temperature study

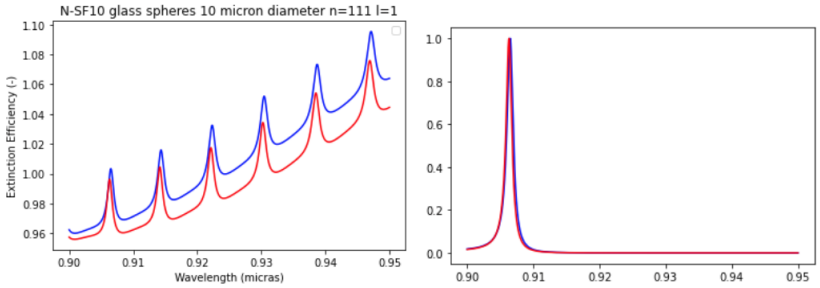

Figure 24: Plot for extinction efficiency and $a_{111,1}$ Mie coefficient for a $10\mu m$ SF10 microsphere immersed in NOA65 for a temperature of 20^oC(blue) and 30^oC(red).

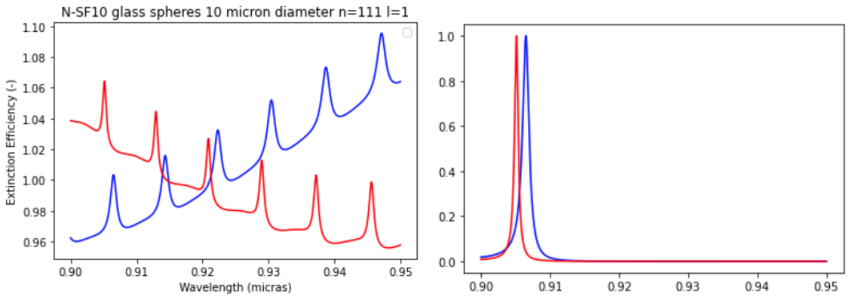

Figure 25: Plot for extinction efficiency and $a_{111,1}$ Mie coefficient for a $10\mu m$ SF10 microsphere immersed in NOA65 for a temperature of 20^oC(blue) and 100^oC(red).

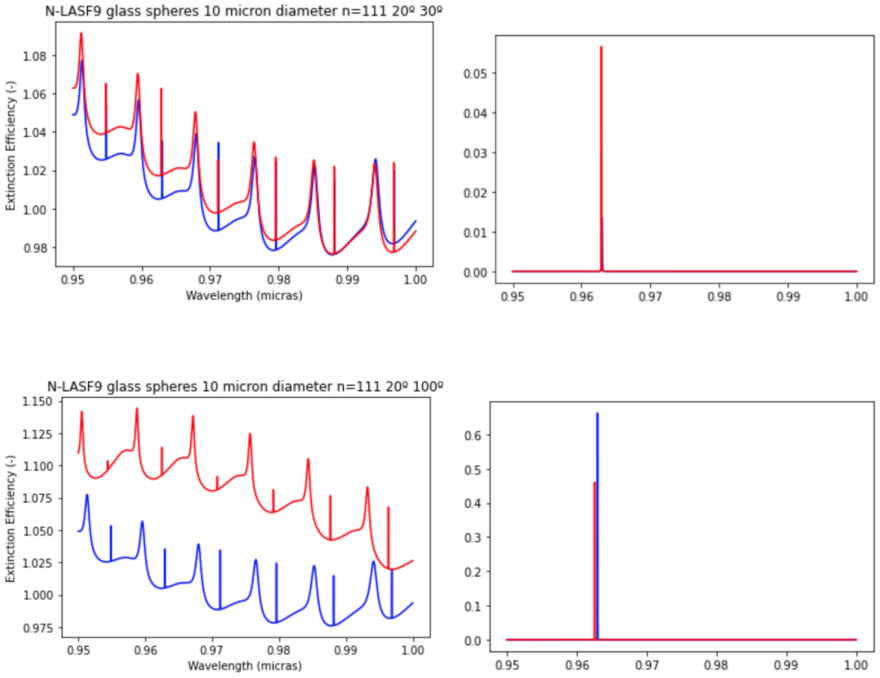

Figure 26: Plot for extinction efficiency and $a_{111,1}$ Mie coefficient for a $10\mu m$ LASF9 microsphere immersed in NOA65 for a temperature of 20^oC(blue), 30^oC and 100^oC(red).

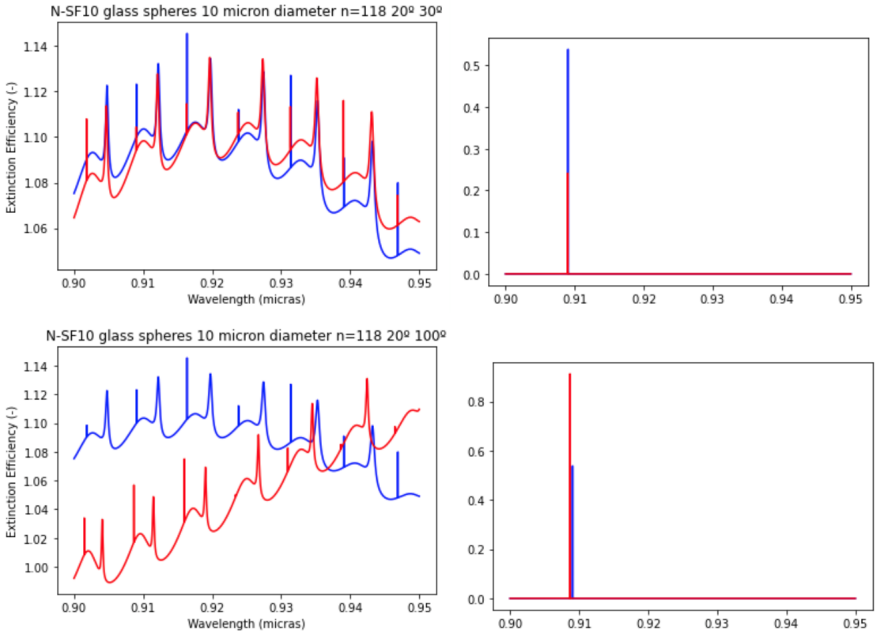

Figure 27: Plot for extinction efficiency and $a_{118,1}$ Mie coefficient for a $10\mu m$ SF10 microsphere immersed in NOA65 for a temperature of 20^oC(blue), 30^oC and 100^oC(red).